ATLAS NOTE

ATL-PHYS-PUB-2006-000

November 12, 2009

A new method to determine the luminosity

The LUCID Collaboration

Abstract

1 Introduction

introduction

The luminosity $\mathfrak{L}$ for a machine delivering pp interactions in bunches can be defined as

$$\mathfrak{L} = \frac{\mu \cdot f_{BC}}{\sigma_{pp}^{inel}} \tag{1}$$

where f_{BC} is the machine bunch crossing (BC) frequency, σ_{pp}^{inel} is the inelastic cross section, and μ is the average number of interactions per BC. In general the average number of interactions per BC is the result of the measurement of one (or, eventually, more detectors) and must be corrected for the detector efficiency ε_{det}. In its turn, the detector efficiency is the weighted average of the efficiency to each process contributing to the pp total inelastic cross section, namely the non diffractive (ND), the single diffractive (SD) and the double diffractive (DD), and therefore one can write

$$\varepsilon_{\text{det}} = \frac{\varepsilon_{ND}\sigma_{pp}^{ND} + \varepsilon_{DD}\sigma_{pp}^{DD} + \varepsilon_{SD}\sigma_{pp}^{SD}}{\sigma_{pp}^{inel}} \tag{2}$$

with self explaining meaning of the used symbols. Therefore, more generally we can write:

$$\mathfrak{L} = \frac{\mu_{\text{det}}}{\varepsilon_{\text{det}}} \cdot \frac{f_{BC}}{\sigma_{pp}^{inel}} = \frac{\mu_{\text{det}} \cdot f_{BC}}{\varepsilon_{ND}\sigma_{pp}^{ND} + \varepsilon_{DD}\sigma_{pp}^{DD} + \varepsilon_{SD}\sigma_{pp}^{SD}} \tag{3}$$

where μ_{det} is the result of the measurement of the average number of interactions per BC by a certain detector. In the present situation of the LHC experiments, in which the inelastic cross section at the 7 GeV/c proton beam momentum has never been measured before, the biggest systematic uncertainty in the determination of the early luminosity measurements will come from the determination of the efficiency, depending heavily on the MonteCarlo (MC) generator adopted. Besides this, another important source of systematic uncertainty comes from the knowledge of the detector response. In the case of LHC, for example, a complete control of the detector response over a wide range of variation of μ is necessary. Also in this case the MC is the main tool used to evaluate systematic uncertainty coming from the response of the detector to multiple interactions. In this respect, a very good description of the event multiplicities of charged and neutral particles is needed, and this is usually achieved only after tuning the MC on data after some training with acquired events. In the following we will describe a method whose aim is reducing the second source of systematic uncertainty above mentioned for the determination of luminosity.

2 MC techniques to simulate a detector response

mc techniques

One of the used technique to simulate a detector response to multiple interactions, consists in overlapping the response of the detector to the single MC generated event. In case of bunched interactions scheme, the events are overlapped following Poisson statistics [1)], and therefore:

$$P(\mu, n) = \sum_{n=0}^{\infty} \frac{\mu^n e^{-\mu}}{n!} \tag{4}$$ eq:poisson

1) We recall here that the two hypothesis which define a Poisson distributed process are:

- The rate at which particles occur over the time must be constant throughout;
- The particles must arrive independently of one another.

where $P(\mu,n)$ is the probability to have n interactions in a *BC*, when the average number of interactions per *BC* is μ. Using this technique the response of a detector to a whatever interaction rate can be measured. The main causes of systematic uncertainty in measuring μ using this method are substantially dependent on the following *MC* accuracies:

1. generator in producing events;
2. simulation in reproducing physics events;
3. detector description;
4. readout description.

Under the assumption of considering a detector with a high degree of stability during the operation time[2] one could think, for studying the response to a whatever μ, to substitute the *MC* sample of single interaction events with a directly measured single interaction data sample. This could be operatively done by requesting special detectors calibration runs for which $\mu \ll 1$ (negligible event pile up) is delivered. The ideal single interaction data sample is reached when the events are triggered with a 100% efficiency device. In this limiting case a *MC* simulation is not any longer needed to predict a detector response to any interaction rate and therefore to measure μ. In case the event trigger efficiency is less than 100% *MC* corrections are needed. Starting with the hypothesis that the response of a detector to a whatever number n of interactions can be built by the response of the same detector to a single interaction, we have developed an original method to measure μ.

3 Description of the proposed method

description

The method is essentially based in two typologies of run which we will name *calibration* and *physics*.

3.1 Calibration runs

calibration

A calibration run is performed at $\mu \ll 1$, that is, in a condition as close as possible to have one interaction per *BC* and to neglect interactions pile-up. The response of a generic detector quantity in this type of runs can be considered as the response to a single interaction. Let's name this response ρ_1 in which ρ identify a measurable quantity (for instance hit multiplicity, total energy , etc.). The response of the detector to any number n of interactions can be built as a linear superposition starting from ρ_1. Let' suppose that in this way we are able to build a set of *reference responses* $\rho_n, n = 1,2,...N_{MAX}$ up to a maximum number N_{MAX} of interactions.

3.2 Physics runs

physics

A physics run is a run performed at an unknown average number of interactions per *BC* (μ) which has to be measured. In case of Poisson *BC* population the frequency of each number of interactions n is coincident with the definition of $P(\mu,n)$ (see Equation eq:poisson 4). As a consequence, the total response R of the detector (for the quantity described by the *reference responses* ρ_n) when the average number of interactions per BC is μ can be expressed as:

$$R = \sum_{n=1}^{N_{MAX}} A \cdot P(\mu,n)\rho_n \tag{5}$$

eq:total res

[2] This assumption is usually quite realistic for well designed detectors having a small number of channels. In case of detectors having a big number of channels, this method could anyway be used by subdividing the detectors itself in many sub parts having a smaller number channels such that the main assumption is well verified.

where A is an eventual normalization factor and the upper limit of the summation, N_{MAX}, has to be suitably chosen in order to make negligible this source of systematic uncertainty.
The theoretical detector response R should then be compared with R_{exp}, the one measured during the physics run. This can be done on statistical basis by fitting the R_{exp} response by means of the R function leaving free the two parameters A and μ. In this way, a direct measurement of μ can finally be obtained. It has to be noticed that, by construction, this method will fail to measure values of $\mu \ll 1$. It will be anyway shown in the following that this method can reliably measure any values of $\mu \geq 0.5$, which are the ones to be considered of practical interest for physics runs.

4 The method applied to the case of the LUCID detector

LUCID (acronym for LUminosity Cerenkov Integrating Detector) is the *ATLAS* detector designed to measure on-line the luminosity delivered by the *LHC* machine and to provide an interaction trigger when running at luminosity up to $10^{32}\ cm^{-2}\ s^{-1}$. A detailed detector description can be found in [1]. The main detecting unit is an Aluminum tube filled with C_4F_{10} radiator gas. When the tube is crossed by a charged particle whose momentum is above the Cerenkov threshold, light is produced and collected at the end of the tube by a photomultiplier tube(*PMT*). The total amount of light produced in a tube is proportional to the number of primary charged tracks produced by the *pp* interactions and crossing the tube. As a consequence, this device allows to count the number of charged tracks per *BC* produced in the interaction point which falls into the detector acceptance the latter being related to the average number of *pp* interactions.The detector consists of two parts, deployed symmetrically around the *ATLAS* interaction point each one consisting of sixteen tubes readout by *PMT*.
LUCID is quite and ideal detector to study the proposed method since its response is characterized by a very good stability on the time scale of days. In the following we will consider two calibration run modes: the first one using the *LUCID* interaction trigger and the second one using an efficient external interaction trigger from the *ATLAS* Minimum Bias Trigger Scintillator *MBTS* system.
In order to evaluate the performances of this method we will use a sample of *MC* data extracted from the ATHENA environment for the *ATLAS* full detector simulation based on GEANT4 [4].

5 Calibration data with LUCID trigger

The calibration data for applying the proposed method to *LUCID* can also be taken by triggering a run with $\mu \ll 1$ with the detector itself.
The main information produced by one *LUCID* channel is a **hit**. If the signal electrical amplitude produced by the collected light is above a certain threshold then one hit is recorded. Usually the threshold is measured in number of photoelectrons *p.e.* produced by the Cerenkov light at the *PMT* photocathode. One charged track above the Cerenkov threshold, crossing the tube axis, produces typically 70 *p.e.* , in the standard detector working conditions (gas absolute pressure 1.1 *bar*). During the first data taking we will start by choosing a threshold value of 50 *p.e.* **for physics runs** to define a hit accordingly to the results of the studies presented in [2]. In the following, we will identify the threshold used to define a hit in the physics runs as thr_{phys}
As a result of the *pp* interactions within one BC, a certain number of hits will be produced on the two detector arms identified in the following as side A and side C. This number can vary from zero to 16 for each detector arm and from 0 to 32 for the full detector. The *LUCID* readout is capable to process the overall number of hits recorded at each *BC* and also to form an interaction trigger from this information. During the calibration runs using the *LUCID* trigger we will require at least one hit detected in each arm of the detector per BC. This trigger scheme will be named as **coincidence mode** and has the evident

advantage to strongly reduce the presence of unwanted events produced by beam halo or background in the calibration runs.
Besides hits, the lucid readout is also capable to record the signal amplitude (proportional to the number of *p.e.*) for each tube for each triggered event. This kind of information can not be used in the on-line processing but is available for the off-line analysis. If the calibration runs (measuring the detector response at the single interaction) are taken by imposing an on-line threshold (in the following named thr_{cal}) on the hits much less than 50 *p.e.*, then, from the amplitudes recorded per each tube and for each trigger event it will be possible to reconstruct with little distortion the total amount of *p.e.* per tube per triggered event for whatever number of interactions.
The effect of applying the hit trigger threshold thr_{cal} during the calibration runs can be appreciated in

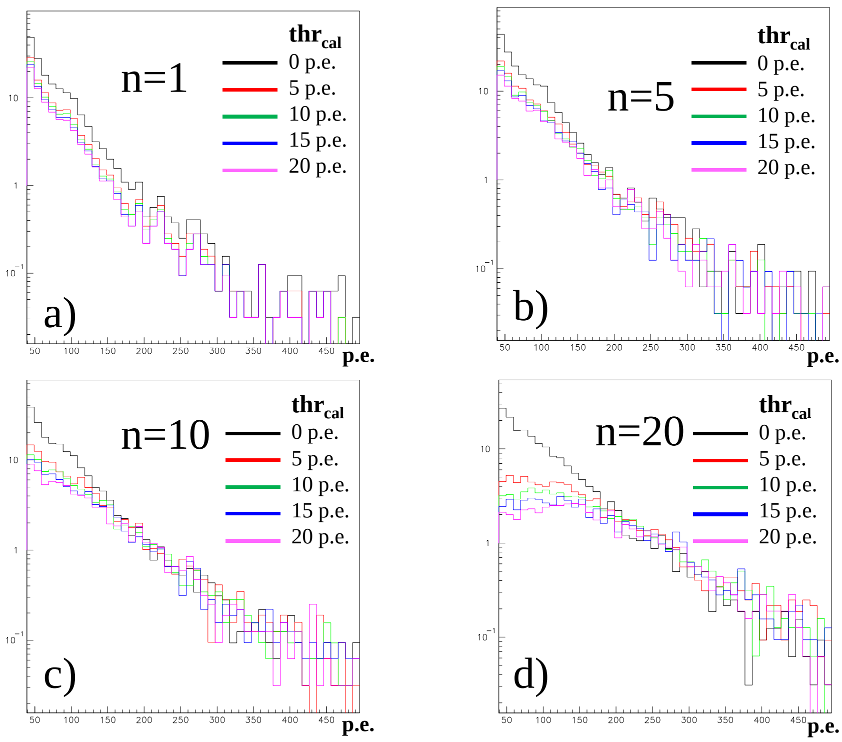

Figure 1: Distributions of the number of *p.e.* per tube per triggered event as a function of the trigger threshold thr_{cal} (in number of *p.e.*) for $n = 1$ interaction (a), $n = 5$ interactions (b), $n = 10$ interactions (c), $n = 20$ interactions (d). The black line distributions represent the limit case reference ones when no trigger threshold is applied.

fig:mixing

Figure fig:mixing 1 where the distributions of the number of *p.e.* per tube per triggered event as a function of the trigger threshold (in number of *p.e.*) are reported for values greater or equal of 50 *p.e.* (the threshold which will be used for physics runs). The completely unbiased distribution with zero *p.e.* threshold (black line) is also shown as a limit case reference. The different distributions are reported for $n = 1$, 5, 10 and 20 interactions. The discrepancy of the distributions with trigger thresholds thr_{cal} greater than zero with respect to the completely unbiased one, increases with the number of interactions. The reason for this is that a trigger threshold greater than zero *p.e.* tends to suppress the low number of *p.e.* part of the distributions. For applying the proposed method to *LUCID* detector we choose, as a **reference responses** ρ_n (see Equation 5) the hit multiplicity distributions per triggered event, which we will denote with $m_n(i)$ where the index n refers to the number of interactions and i is the overall multiplicity per triggered event recorded by *LUCID*. The index i can effectively run from 2 to 32 hits, the lower value being constrained by the coincidence mode. The reference responses $m_n(i)$ are built by applying the thresholds which will be used in the physics runs (for example $thr_{phys} = 50$ *p.e.*) to the distributions of the number of *p.e.* per tube per event similar to the ones reported in Figure 1. In Figure 2 four examples

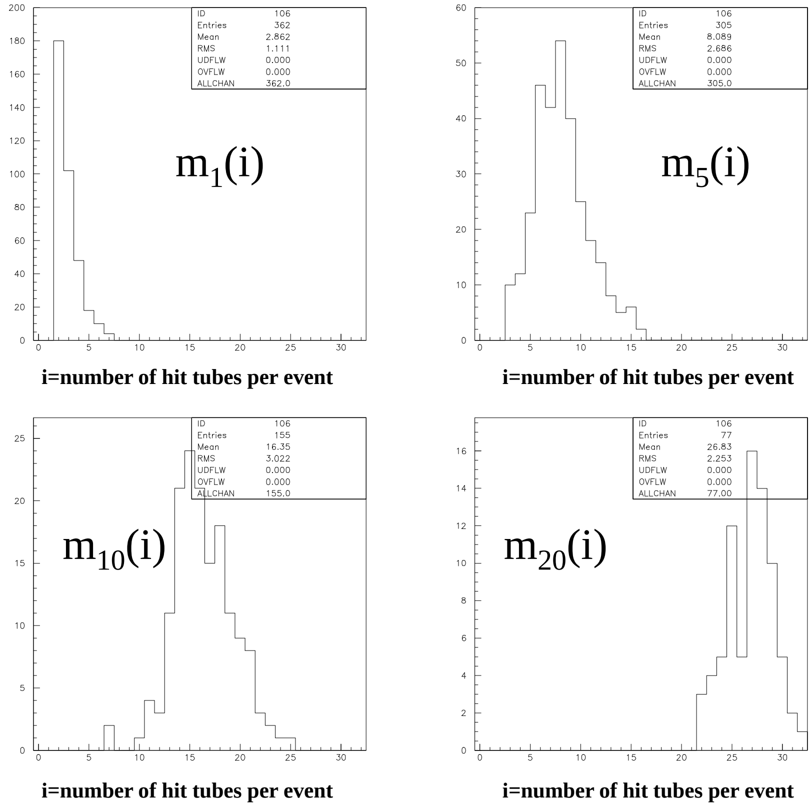

fig:mni

Figure 2: Examples of reference responses $m_n(i)$ for $n = 1$, 5, 10 and 20 interactions. The trigger threshold in the calibration runs is set at $thr_{cal} = 10$ *p.e.* and in the physics runs at $thr_{phys} = 10$ *p.e.* .

of reference responses $m_n(i)$ built using $thr_{cal} = 10$ *p.e.* and $thr_{phys} = 50$ *p.e.* are shown.

6 Systematic uncertainties with data triggered by LUCID

systematic

7 Applying an external trigger

ExtTrig_App

Because of the need to introduce a calibration threshold cut (thr_{cal}) when using LUCID as a trigger, some bunch crossings will be detected while others will be left undetected. In order to build a realistic

LUCID response to bunch crossings with multiple interactions from the reference samples, it is necessary to know the response of LUCID to undetected bunch crossings. An external trigger could be used in combination with lucid to provide such a sample of *unbiased single interactions* from the calibration runs. This is possible since an external trigger would be able to select those events, in which LUCID detects some activity but not a large enough signal to separate the signal from general background/noise. For this study the Minimum Bias Trigger Scintillators (MBTS) have been chosen to provide the external trigger. Other detector system could in principle also be used but the MBTS was chosen since it is designed to efficiently detect min bias events. This high efficiency combined with the fact that the min bias events constitutes the bulk part of the total inelastic cross section makes the MBTS a ideal candidate to provide a unbiased trigger for the calibration runs. Another motivation for using an external trigger is to minimize the influence of systematic uncertainties on the calibration constant. This will be described in greater detail in sec. 9

The MBTS consistes of sixteen scintillator counters installed on the inner face of the end-cap calorimeter cryostats. Each set of counters is segmented in eight units in ϕ and two units in η. They are located at $|z|$ = 3560 mm, the innermost set covers radii between 153 mm and 426 mm, corresponding to the region $2.82 < |\eta| < 3.84$ and the outermost set covers radii between 426 mm and 890 mm, corresponding to the region $2.09 < |\eta| < 2.82$. The MBTS were designed to function only during initial data-taking at low luminosities. After 3-4 months of higher luminosity operation the scintillators will yellow due to radiation damage. Systematic uncertainties due to degrading MBTS performance will be discussed in sec. 9.3

As mention in sec. 5 all trigger in this study are used in coincidence mode. At the level of the level 1 trigger (LVL1) this means that hit above a certain threshold has to be recorded at each side within the same BC for the trigger to fire. For the MBTS the threshodls is nominal threshold is set to 40 mV. The efficiencies for the triggers used in this analysis are given in table 7.

tab:trigeff

LVL1 trigger item	ND	SD	DD
L1_MBTS_1_1	$99.5 \pm 0.7\%$	$44.2 \pm 2.8\%$	$53.5 \pm 2.6\%$
L1_LUCID_A_C	$28.5 \pm 3.7\%$	$1.0 \pm 686.9\%$	$2.1 \pm 269.5\%$

Table 1: Level 1 trigger efficiencies for the non-, single and double-diffractive data sets used in this analysis. The large uncertainties on the LUCID items are due to lack of statistics since the efficiencies for the items are quite low.

One of the main motivations for running the triggers in coincidence mode is to suppress contribution from background events. Especially two sources related to the beam background are believed to give significant contribution to the signal , namely beam gas and beam halo events. The influence of the on the LUCID response from these two sources of background will be discussed further in sec. 9.4.

8 Calibration of data using an external trigger

ExtTrig_Cal

As described above the external trigger is only intended to be used in the calibration runs. The reason for the this is as also mentioned above, to provide a sample of *unbiased single interactions* from the calibrations runs. Since the aim of the physics runs is to provide the response in LUCID to a unknown number of collisions and not to a single interaction the external trigger is not needed in the physics runs. Figure 3(a) show the distribution of number $p.e$ per tube as recorded in LUCID when it is required that the event is detected by the external trigger. Its is clearly seen from the curves for both non-diffractive (black points) and diffractive (red and blue points) events that that using a external trigger does not remove the characteristics of the signal. This could potentially have been the case if a trigger with a strong bias

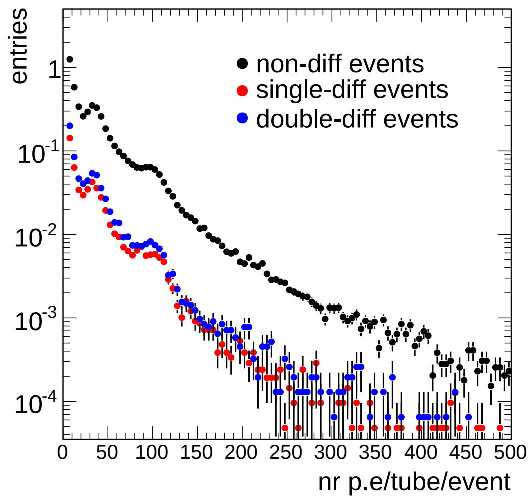

(a) Photo-electron distribution in the reference sample

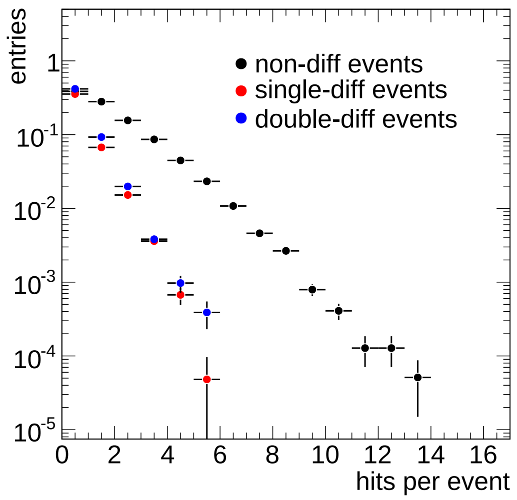

(b) hits per events distribution in the reference sample

Figure 3: Figure 3(a) shows the distribution of number *p.e* per tube per event triggered by the MBTS trigger in coincidence mode. Figure 3(b) shows the distributions of avarage number of hits in LUCID in events triggered by the MBTS. The definition of a hit is as mentioned earlier a signal a above 50 p.e. In both plots the histograms are normalized to the same number of events.

were chosen as a external trigger instead of the minimal biased trigger provided by the MBTS system. Both the distribution from the non-diffractive events and the two components of the diffractive events exhibits clear peaks at the expected positions. A peak near 30 p.e is expected from the signal of particles transversing the quartz window of PMTs and not the gas. Also one would expect to see a peak near 100 p.e from particles produced at the interaction point transversing both the gas as well as the quartz window (*ref to test beam paper?*). The smaller number of entries in the distributions form single and double diffractive events as compared to the distribution from the non-diffractive events is due to two effects. Firstly, since the distributions shown in the plots is obtained from events triggered by the MBTS, the distributions will be convoluted by the efficiency curve of the MBTS. Since the MBTS trigger efficiency curve for detecting a diffractive event is flat in p_T , η and lower than for a non-diffractive events this effectively amounts to a downscaling of the distribution. Secondly, the fact that non-diffractive events in general have a larger charged multiplicity in the eta acceptance of LUCID [5]. The latter is also clearly seen from figure 3(b) where the average number of hits for non-diffractive and diffractive events are compared. When using the an external trigger instead LUCID itself as a trigger the sample from which the plots in 3(a) are generated serves as the reference sample from which the reference responses $m_n(i)$ are build. It is therefore important to check that the sample exhibits the same essential features a the sample obtained in the physics runs. This will ensure us that the reference sample obtained by using an external trigger is truly the most unbiased sample one can obtain.

To extract the value of μ_{meas} from a certain experimental response a weighted sum of the reference responses , namely the theoretical detector response $R(\mu)$ (see eq. 5) is fitted to $R_{exp}(\mu)$. Examples of such fits are shown in 4(a) for four different values of n. Both reference sample as well as the physics samples (poisson statistics) used to generate these plots are a mixture of non-diffractive and diffractive events to mimic a sample inelastic events. In this study the inelastic MC sample consist of 70 % non-diffractive events and 18 and 12 % single and double diffractive events respectively. Since the actual fraction of non-diffractive and diffractive events in inelastic events are not fully known this will contribute

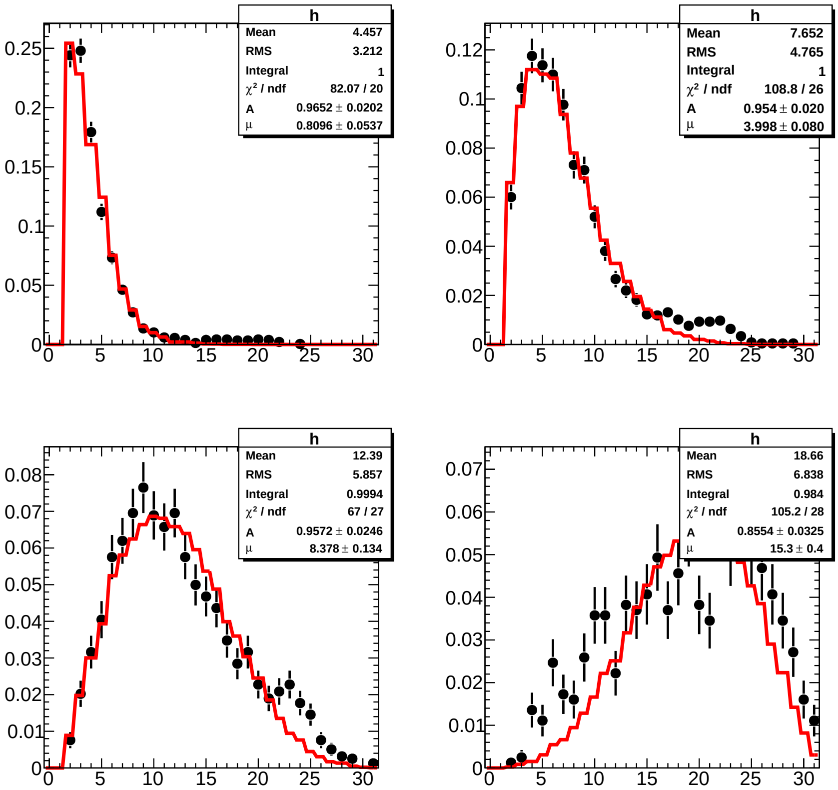

Figure 4: Examples multiplicity distributions from the physics runs for four different values of $n = 1,5,10,20$. The red line shows fits of the LUCID response function $R(\mu)$ multiplicity distributions $R_{exp}(\mu)$.

to the systematical uncertainties as discussed in greater detail in sec. 9.1.
Once μ_{meas} has been obtained from the experimental detector responses $R_{exp}(\mu)$ for a suitable range of μ, the calibration constant κ_{MC} for the data set can be extracted. This is done by plotting the measured values of μ as a function of the true value and fitting the resulting curve with a 1st polynomial trough the origin. Figure 5(a) shows such a fit to the values of μ_{meas} for the total inelastic data set (red dots). The dotted black line shows a one-to-one correspondence between μ_{meas} and μ_{true}. To illustrate the need for a calibration of the data the deviation between the measured and true value of μ , $(\mu_{meas} - \mu_{true})/\mu_{true}$ are plotted as a function of μ_{true} in figure 5(b) . In the hypothetical situation where the fitted line had been coincident with the one-to-one line[3)] the need for a calibration constant would disappear . In that case the data would be self calibrated. Table 8 gives the calibration constant for the different components of the inelastic data set and for the inelastic data set itself.
Just as the total luminosity can be calculated from the contributions of the non-diffractive and diffractive parts *(ref to marco eq 3)* so can the calibration constant :

$$\kappa_{MC}^{inel} = \frac{\varepsilon_{ND} f_{ND} \kappa_{MC}^{ND} + \varepsilon_{SD} f_{SD} \kappa_{MC}^{SD} + \varepsilon_{DD} f_{DD} \kappa_{MC}^{DD}}{\varepsilon_{inel} f_{inel}} \qquad (6)$$

[3)] $(\mu_{meas} - \mu_{true})/\mu_{true} = 0$ for all μ_{true}

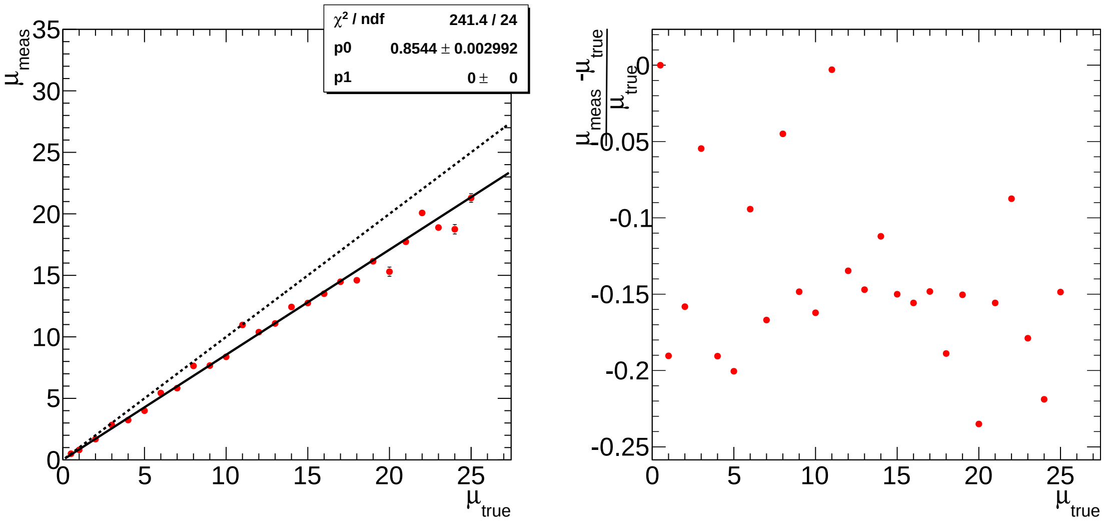

(a) μ_{meas} vs μ_{true} (b) Absolute deviation of μ_{meas} from μ_{true}

Figure 5: The red data points on figure 5(a) shows the measured values of μ as a function of the true value for the total inelastic data set. The solid black line in the plot shows result of linear fit to the data points. The dotted black line shows a one-to-one correspondence between μ_{meas} and μ_{true} . Figure 5(b) shows the absolute deviation of μ_{meas} from μ_{true} as a function of μ_{true}

where f_i is the fraction of events of type i in the total inelastic data set ($f_{inel} = 1$). ε_i denotes LVL1 trigger efficiency for data set i and κ^i_{MC} is the calibration constant for data set i. Inserting the numbers from table 8 and table 7 one can calculate that expected value of κ^{inel}_{MC} for the total inelastic data set to be 0.89. This value is only a little higher than the measured value which is 0.85.

tab:kmc

event type	ND	SD	DD	inelastic
κ_{MC}	0.932 ± 0.002	0.682 ± 0.007	0.792 ± 0.006	0.854 ± 0.003

Table 2: Calibration constants for the different data sets considered in this analysis.

One of the main feature of the method presented here is that it yields a linear relation between μ_{meas} and μ_{true}. This feature is intrinsic to the method and other methods/algorthms might not display the same feature. In this case the method is based on evaluation of a *calibration curve* [2] instead of a calibration constant. As a general trend the fewer parameters the calibration curve contains the more predictive the method is. This means that a linear method like one presented here only needs one calibration point apart from the origin to predict the luminosity in the full LHC range. It is assumed that at zero interaction per BC that the measures value of μ will also be zero. Whether or not this is a fair assumption will be discussed in sec. 9.4 where the influence of beam background is addressed.

9 Systematic uncertainties with data triggered by external device

ExtTrig_Sys

The following section aims to describe in detail some of the sources of systematic uncertainty contributing to the overall uncertainty. The largest contributions are foreseen to stem from changes in running conditions between the calibration runs and the physics runs. It is a fundamental assumption of the method is that any set of calibration and physics runs can be carried out under the same running conditions. If this is not the case then a bias will be introduced on μ_{meas} by potential having different shapes of the multiplicity distributions in the two data taking scenarios. Finally, the method assumes a Poissonian distributed number of collisions per bunch crossings. Any deviation from this behavior may cause loss in accuracy. Monte Carlo simulations are used to evaluate the impact of systematic uncertainties on the ability to extract the calibration constants and luminosity. The way that the impact of the systematic uncertainties are uncovered here is by investigating all main contributions from the different sources. As mentioned is expected that the main source of systematic uncertainty will arise by unintended changes in the running conditions between the calibration and physics runs. In the following sections the effects of such changes will be investigated by systematically changing the running conditions between the calibration and physics runs. A difference in the ratio of diffractive (SD+DD) to non-diffractive events (ND) between the two runs types is expected be such a source of systematic uncertainty. Bunch per Bunch variations in μ_{true} might also have an effect. Also a change in the in trigger conditions between the calibration and physics runs is expected to have an impact.

9.1 Composition of data sets

sec:mixture

Since the average charged multiplicity is higher for non-diffractive events than for diffractive events [5] it will lead to a shift in μ_{meas} if the composition of the calibration and physics run is not identical. As the difference in charged multiplicity between single and double diffractive events are not as significant as the difference between the non-diffractive and diffractive events, only a difference in ratio between the two latter in the calibration and physics data sets will potentially lead to a shift in μ_{meas}. Figure 6(a) show how the value of κ_{MC}^{inel} changes as the fraction of non-diffractive events in the reference sample is changed. From the plots is clearly seen that as the fraction of diffractive events in the reference samples gets larger the value of κ_{MC}^{inel} gets smaller. This is expected since as the fraction of diffractive events in the reference gets larger the average multiplicity per event will decrease leading to a smaller value of μ_{meas}. The contribution of this effect to the systematic uncertainty is estimated to be $\approx 2\%$

As mentioned before the inelastic data sets consist of 70 % non-diffractive events and 18 and 12 % single and double diffractive events. Since the actual fraction of non-diffractive and diffractive events in inelastic events are not fully known and it has be checked if the value if the value of κ_{MC}^{inel} depends on the overall composition of the data sets. Figure 6(b) shows the value of κ_{MC}^{inel} as a function of changes to the overall event composition of the data sets. The contribution of this effect to the systematic uncertainty is estimated to be $\approx 3\%$

Traditionally also central diffractive events (CD) belongs to the category of diffractive events. However since the central diffractive cross section constitutes less than 1 % of the total inelastic pp cross section, these events have been ignored in this study.

9.2 Bunch to bunch variation in μ_{true}

unchtobunch

Apart form the event composition for the data sets also variations in number of collisions per BC might also have an influence on the calibration constant. In the physics runs it is assumed that the number of collisions per BC is poissonian distributed around μ. However situations may occur where the true value of μ is subject to a systematic shift. In such situations the value of μ_{true} form the physics runs and the calibration runs will not be equal and as a results the value of the κ_{MC} will be shifted compared to the true value. However it is a imbedded feature of the method presented here that the shift in κ_{MC} is directly proportional to the actual shift in μ_{true}. Since such shifts are only expected to occurs in less than 1 %c of the bunch crossings the contribution of this effect to the systematic uncertainty is estimated to be $< 1\%$

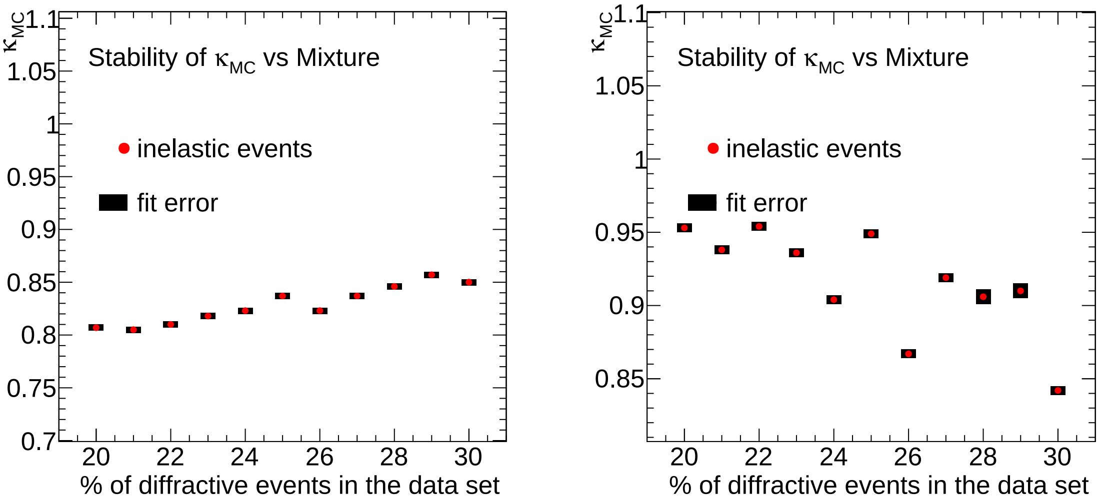

(a) κ_{MC}^{inel} vs change in % of diffractive events in the reference sample

(b) κ_{MC}^{inel} vs change in % of diffractive events both samples

Figure 6: Value of κ_{MC}^{inel} as a function of changes in the fraction diffractive events in the data set. In figure 6(a) only the composition of the reference is modified. In 6(b) the composition of both the reference sample as well as the physics are modified.

9.3 Trigger conditions

As mentioned before the method presented here requires stable running conditions. Stable in this case means that the running conditions between the calibration runs and the physics runs can not change considerbly.
As can be seen from the table 7 the LVL1 efficiencies for the MBTS to detect a inelastic interaction are high, even in coincidence mode. However this might changes as the scintillators will start to yellow due to radiation damage. Over time this will diminish the amount light that can be read out and as a result the gain of the PMTs has to be increased. To cope with the higher noise level due to the increased gain, the threshold on the readout electronics will have to be increased accordingly. Operationally wise for the MBTS an increase in threshold will lead to a decrease in trigger efficiency. Since the external trigger is only used in the calibration runs it is important to investigate if changes to the external trigger efficiency will introduce a bias to the reference sample and thereby modify κ_{MC}. Figure 9.1 displays the stability κ_{MC} for the total inelastic data set when the MBTS threshold is changed. As can be seen from the figure the value of the calibration constant fluctuates around a central value of 0.87 when the MBTS threshold is increased form the nominal value of 40 mV to 1V. Above this value the trigger electronics of the MBTS saturates and the threshold can not be raised further. However raising the threshold all the way up to 1V is a very unlikely and unphysical situation. A more likely scenario is a change of the threshold of about 25 % from the nominal value. Since a change of 25 % to the MBTS results in a 1 % variation in κ_{MC} is is estimated that the contribution of this effect to the systematic uncertainty is 1%
The fluctuations in κ_{MC} in figure. 9.1 does raise an important question. Will a change in efficiency of the external trigger introduces a bias into the reference samples. As mentioned before the MBTS was chosen to since it is the best candidate to provide a unbiased external trigger. Changing the running condition for MBTS by changing the threshold could potentially change this. Whether or not this is the case can be investigated by comparing the shape of the reference histograms taken with and without the external

g:kmcvsmbts

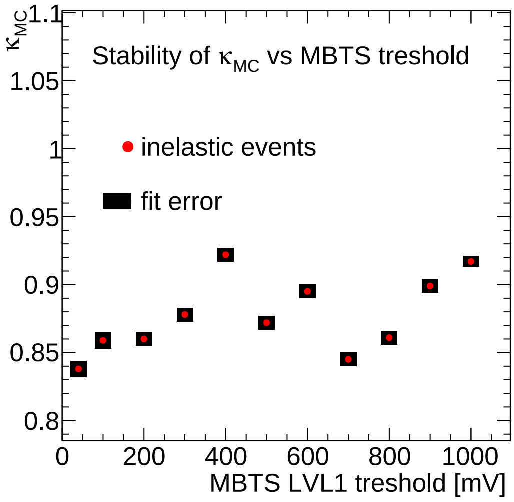

Figure 7: Value of κ_{MC}^{inel} as a function of changes to the MBTS threshold.

trigger for different values of the MBTS threshold. Such a study reviles that the relative difference in RMS and mean value between the reference histograms taken with or without the MBTS for different values of the threshold, is less than 1 %. It can therefore be concluded that changing the trigger threshold for the MBTS does not introduce a bias to the reference samples.

9.4 Background

sec:beambck

The main backgrounds in minimum bias events, particularly during early running, will be beam-gas collisions within the beampipe over the length of ATLAS, and beam-halo from interactions in the tertiary collimators in the accelerator. It is important to take these events into considerations since they have the potential of providing spurious triggers. So in order not to pollute the total inelastic data set, beam background events must be filtered out. During early low luminosity running a large fraction of bunch crossings will have no pp interaction. Using a trigger based only on bunch-crossings would result in a large number of empty events, which only contain detector noise, being recorded. Therefore, the trigger must be able to reject such events in order to optimise the use of the trigger bandwidth.
The beam background will most like not contribute significantly to the signal during the physics runs where the rate of beam background to signal events are kept low. However this might not be the case in the calibration runs where $\mu << 1$ resulting in a higher beam background to signal event ratio. Given the inelastic nature of the beam gas event the MBTS will unavoidably of have a high efficiency to detect these kind of events. This means that using the MBTS as an external trigger during the calibration runs will introduce a larger fraction of beam background into the reference samples, than to the ones taken in the physics runs. To judge whether or not beam background events can be successfully filtered out the characteristics and rates of the background events needs to be assessed in comparison with the signal events. In the sections below the contributions from beam gas and beam halo events will be addressed separately.

9.4.1 Beam gas events

Beam-gas interactions along the experimental insertion regions have been indentified as one of the main sources of background to the experiments in the LHC. In the LHC the main gas species are expected to

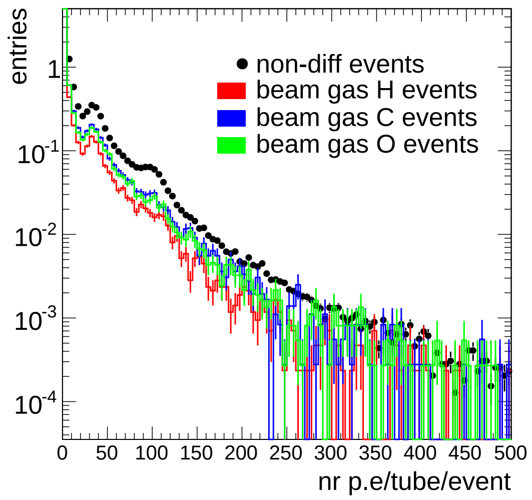

(a) Photo-electron distribution for non-diffractive and beam gas events

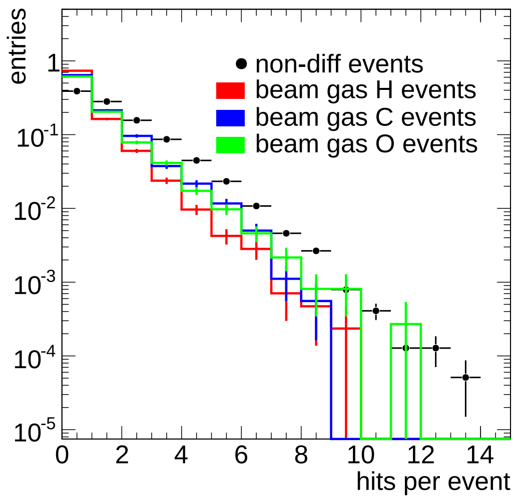

(b) Hits per events distribution for non-diffractive and beam gas events

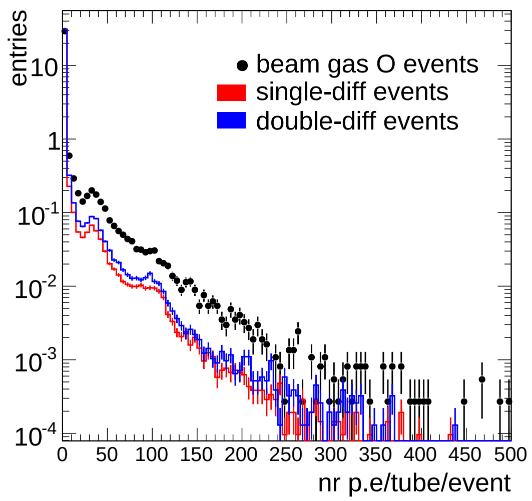

(c) Photo-electron distribution for diffractive and beam gas events

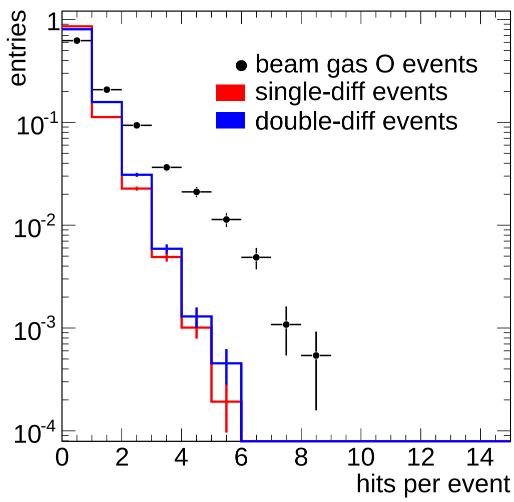

(d) Hits per events distribution for diffractive and beam gas events

Figure 8: Comparison between the Photo electron and hits per event distributions for signal and background events. Figure 8(a) and 8(b) and shows a comparison of the photo-electron and hits per event distribution for non-diffractive events and the different components of the beam gas events. Figure 8(c) and 8(d) shows a comparison of the photo-electron and hits per event distribution for one components of the beam gas events and the different components of the diffractive events . All the histograms shown in the plots above are normalized to the same number of events

be hydrogen (largely dominant in the cold arcs), methane, carbon monoxide and dioxide. The presence of water should be negligible, given that room temperature sections are conditioned (baking and NEG activation), and that the water will have an extremely low vapour pressure in the cold sections.
Figure 8(a) and 8(b) and shows a comparison of the photo-electron and hits per event distribution for non-diffractive events and the different components of the beam gas events. Figure 8(c) and 8(d) the

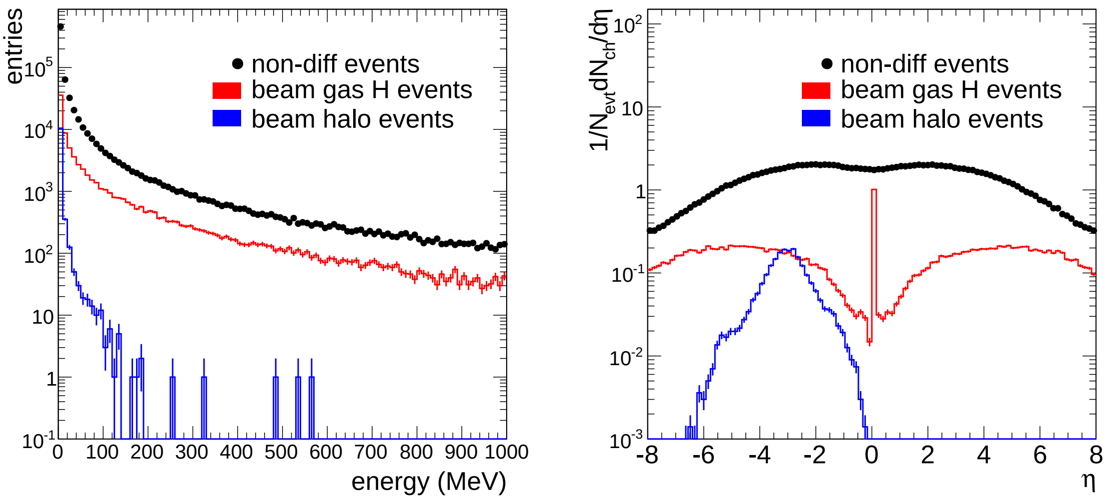

(a) Energy distribution for charged particles.

(b) Rapidity distribution for charged particles.

Figure 9: Generator level comparison of the energy and changed multiplicty distribution for non-diffractive, beam gas and beam halo events.

same kind of comparison but this time for one components of the beam gas events and the different types of the diffractive events. As can be seen from the plots, the characteristics in term signals in the PMT's or average multiplicity are not significantly different in the beam gas events as compared to the signal events. . The overall shape of the photo-electron spectra for the beam gas events are similar to those of the signal events although the expected peak at 100 p.e seems to be less pronounces. Also the hits per event distributions for the beam gas events seems to be very similar to those of the signal events with a average multiplicity somewhere in between the non-diffractive and the diffractive events. This is most likely due to the inelastic nature of the beam gas interactions, which brings us to the conclusion that it is not possible to filter out the beam gas events by implementing cuts based on signal characteristics in LUCID.

tab:trigeffbeamback

Table 9.4.1 show the Level 1 trigger efciencies for beam gas and beam halo events. Based on the

geffbeamback

LVL1 trigger item	beam gas H	beam gas C	beam gas O	beam halo
L1_MBTS_1_1	$36.1 \pm 8.3\%$	$43.6 \pm 6.9\%$	$43.6 \pm 6.9\%$	$<< 1\%$
L1_LUCID_A_C	$0.3 \pm 116.64\%$	$0.6 \pm 327.4\%$	$0.7 \pm 280.1\%$	$<< 1\%$

Table 3: Level 1 trigger efficiencies for beam gas and beam halo events.

numbers in the table and assuming that beam gas consists of 17 % hydrogen , 29 % carbon and 54 % oxygen [6] beambackground1 is can be calulated that the overall efficiency to detect a beam gas events is 42.3 % for MBTS LVL1 trigger and 0.6 % for the LUCID LVL1 trigger. The low efficiency for the LUCID combined a expected beam gas rate of 4 Hz at start-up [6] beambackground1 leads us to the conclusion that the contribution from beams gas events is negligible. The contribution to the systematical uncertainty is estimated by including beam gas events into to the total inelastic data in rates proportional to the beam current. Going from 4 Hz at start-up/calibration runs to 0.4 kHz at nomunal luminosity. The induced changes in the calibration constant is $<< 1\%$ hence the systematics from beam gas events can be ignored. It should be noted that a *time-of-flight* cut might suppress the beam background rates futher. However such a cut has not been used in this study.

9.4.2 Beam halo events

"Beam halo" events occur as a single beam of protons is circulating in one direction in LHC, just passing through ATLAS. An outlier particle hits a part of the detector causing a spray of particles. Such events will in general have a soft energy spectra and low charged multiplicity compared to inelastic events as can be seen from 9(a) and 9(b). As it can be seen from 9(a) a large of the particles produced in a beam halo event will lie below the cherenkov threshold. Combined with the one-sided topology of the beam halo events (see figure. 9(b)) this means that LVL1trigger efficiency for LUCID is very low (see table 9.4.1) and as a result the conclusion is that the contribution from beam halo events can safely be ignored in this study.

10 Summary and conclusions

sec:summary

10.1 Evaluation of the total systematics

tab:sys

	intrinsic trigger		external trigger	
Quantity	$\pm\Delta Q/Q$	$\pm\Delta\kappa_{MC}/\kappa_{MC}$	$\pm\Delta Q/Q$	$\pm\Delta\kappa_{MC}/\kappa_{MC}$
(SD+DD)/(SD+DD+ND)	25%	6%	25%	2.5%
Thr1	20%	3%	20%	1%†
Thr2	20%	<1%	20%	<1%
bunch to bunch variation in μ_{true}	25%	2%	25%	<1%

Table 4: Comparison between the estimated systematics when using a intrinsic and external trigger in the calibration run. † when using an external trigger thr1 is replaced by a threshold cut specific to the detector system used as a trigger.

11 Acknowledgements

References

atlas [1] The *ATLAS* Collaboration, G. Aad et al., The *ATLAS* Experiment at the CERN Large Hadron Collider, JINST 3 (2008) S08003.

antonello [2] The *LUCID* Collaboration, Simulation of Luminosity Monitoring with LUCID in ATLAS, ATLAS Note 2009-xx.

athena [3] ATLAS Collaboration, CERN-LHCC-2005-022 (2005).

geant4 [4] S. Agostinelli et al., Nucl. Instrum. Meth. A 506 (2003) 250-303.

minbias [5] The *ATLAS* Collaboration, Expected Performance of the ATLAS Experiment, CERN-OPEN-2008-020

nbackground1 [6] A. Rossi. Estimates of the residual gas density in the LHC. LHC Workshop on Experimental Conditions and Beam-Induced Detector Backgrounds

nbackground2 [7] V. Talanov, Estimation of the machine induced background for the commissioning period with tertiary collimators in the IR1 of the LHC ,LHC Project Note 371, 2005